Longitudinal *in vivo* coherent anti-Stokes Raman scattering imaging of demyelination and remyelination in injured spinal cord

Yunzhou Shi
Delong Zhang
Terry B. Huff
Xiaofei Wang
Riyi Shi
Xiao-Ming Xu
Ji-Xin Cheng

Longitudinal *in vivo* coherent anti-Stokes Raman scattering imaging of demyelination and remyelination in injured spinal cord

Yunzhou Shi,[a,*] **Delong Zhang,**[b,*] **Terry B. Huff,**[b,*] **Xiaofei Wang,**[c] **Riyi Shi,**[a,d] **Xiao-Ming Xu,**[d] **and Ji-Xin Cheng**[a,b]
[a]Purdue University, Weldon School of Biomedical Engineering, West Lafayette, Indiana 47907
[b]Purdue University, Department of Chemistry, West Lafayette, Indiana 47907
[c]Indiana University School of Medicine, Spinal Cord and Brain Injury Research Group, Stark Neurosciences Research Institute and Department of Neurological Surgery, Indianapolis, Indiana 46202
[d]Purdue University, Department of Basic Medical Sciences and Center for Paralysis Research, West Lafayette, Indiana 47907

Abstract. *In vivo* imaging of white matter is important for the mechanistic understanding of demyelination and evaluation of remyelination therapies. Although white matter can be visualized by a strong coherent anti-Stokes Raman scattering (CARS) signal from axonal myelin, *in vivo* repetitive CARS imaging of the spinal cord remains a challenge due to complexities induced by the laminectomy surgery. We present a careful experimental design that enabled longitudinal CARS imaging of de- and remyelination at single axon level in live rats. *In vivo* CARS imaging of secretory phospholipase A$_2$ induced myelin vesiculation, macrophage uptake of myelin debris, and spontaneous remyelination by Schwann cells are sequentially monitored over a 3 week period. Longitudinal visualization of de- and remyelination at a single axon level provides a novel platform for rational design of therapies aimed at promoting myelin plasticity and repair. © *2011 Society of Photo-Optical Instrumentation Engineers (SPIE).* [DOI: 10.1117/1.3641988]

1 Introduction

Understanding the activity of cells in the central nervous system (CNS) *in vivo* represents a frontier of neuroscience. With sub-cellular resolution and high-speed imaging capability, *in vivo* fluorescence imaging has permitted visualization of neurons in the brain[1] and optic nerve.[2] Additionally, fluorescence imaging has shown the time course of axon degeneration and regeneration[3] and enabled quantification of vascular and axonal network reorganization[4] after a spinal cord injury. Though much attention has been paid to neurons, *in vivo* imaging of myelin sheath, which comprises 50% of the dry weight of CNS white matter, remains difficult.

The myelin sheath is a multilayer membrane which wraps axons in the nervous system to provide electrical insulation and enable high-speed impulse conduction. Demyelination is a hallmark of CNS disorders such as spinal cord injury and multiple sclerosis.[5,6] Promoting myelin regeneration is essential for re-establishing a function to the injured spinal cord.[7] Although many potential treatments are under investigation,[8] difficulty in optimizing treatment parameters and an incomplete understanding of the mechanisms behind these therapies hinders their translation into clinical use. Such difficulties are partly due to limitations in technologies available. Histology and electron microscopy allow direct visualization of myelin,[5,9] but sample fixation and staining preclude *in vivo* studies in the same animal. Electrophysiology and behavioral assessment help evaluate axonal conduction and locomotor function,[10] but cannot visualize spinal cord constituents that contribute to conduction loss or improvement. *In vivo* imaging techniques such as MRI and PET lack the spatial resolution to visualize single myelin,[11,12] limiting their application to whole tissue studies.

Coherent anti-Stokes Raman scattering (CARS) microscopy has made possible label-free and high-speed imaging of myelin sheath with three-dimensional sub-micron resolution[13] and has been employed to explore the mechanisms of demyelination induced by lysophosphatidyl choline[14] and glutamate excitotoxicity.[15] Additionally, CARS has been utilized for intravital imaging of axonal myelin in the sciatic nerve.[16,17] However, longitudinal *in vivo* CARS imaging, especially for the spinal cord, has been hindered by several challenges including 1. invasive surgical procedures to expose the cord for imaging with a traditional microscope objective complicate animal survivability, 2. motion of the spinal cord tissue arising from the animal's respiration and heart-beat results in image distortion, 3. blood deposition on the spinal cord reduces optical penetration, and 4. scar-tissue formation complicates subsequent exposure of spinal tissues. By overcoming these obstacles, we demonstrate *in vivo* repetitive CARS imaging of spinal cord myelin. Furthermore, we show the potential of our method for remyelination studies by longitudinal CARS imaging of myelin degradation and regeneration in the same rats over a period of

3 weeks in a group III secretory phospholipase A$_2$ (sPLA$_2$-III) induced demyelination model.

2 Experimental Section

All procedures (see Video 1) performed were approved by the Purdue Animal Care and Use Committee. Long-Evans or Sprague Dawley rats (200 g) were anesthetized by intraperitoneal injection of Ketamine/Xylazine (90 mg/kg Ketamine, 9 mg/kg Xylazine). Once the animals were deeply anesthetized, the spine was exposed by making an incision through the skin and muscle tissue at T10, where the natural curvature of the spinal cord makes this region more superficial to the skin than other locations, reducing the amount of tissue that needs to be removed to expose the cord, thereby improving the survivability and recovery time of the animals. For imaging with a MicroProbe Objective (MPO, Olympus), after the vertebrate bone was exposed, a small drill was used to form a 2-mm diameter concave in T10 to expose the spinal cord. The hole was filled with sterile saline to keep the tissue hydrated and to serve as an immersion medium for MPO. For imaging with a $40\times$ water immersion objective, the spinal cord was exposed by dorsal half-laminectomy at T10. To induce local demyelination, 0.2 μL of group III secretory phopholipase A$_2$ (sPLA$_2$-III)[18,19] (3 to 6 ng in sterile saline, Sigma, St. Louis, Missouri) was injected into the spinal cord beneath the pia mater using a 10 μL Hamilton syringe and the needle was left in place for 1 min to allow for diffusion into the tissue. Control animals received a 0.2 μL injection of sterile saline. Before the animal recovered from surgery, a cushion of agarose gel was formed above the exposed spinal cord by applying a warm solution of agarose (3% in sterile saline) dropwise onto the cord until the cavity created by a laminectomy had been filled. After the imaging procedure, the rats were subcutaneously injected with analgesics (Buprenorphine, 0.05 to 0.1 mg/kg) every 12 h for 3 days following the surgery.

3 Results and Discussion

Our imaging study was carried out on an upright CARS microscope (see Video 1), which is depicted in Ref. 20. Using the miniature microscope objective ($20\times$ MPO, 0.5 N.A., Olympus) shown in Fig. 1(a) left panel, we performed high-resolution CARS imaging of parallel myelin fibers of the superficial dorsal funiculus while reducing the surgery necessary for imaging. We obtained a comparable image quality with the miniature objective [Fig. 1(b)] as that seen with a water immersion $40\times$ objective [LUM PlanFl/IR, N.A. = 0.8, Olympus, Fig. 1(c)]. For the rest of the experiments we used the $40\times$ objective [Fig. 1(a), right panel] which provides a much larger working distance (3.3 mm) than the miniature microscope objective (200 μm). Following exposure of the spinal cord, we stabilized the spine by a custom clamping system [Fig. 1(a)] which allowed the animal to breathe freely. Without spinal stabilization, CARS imaging suffered from motion induced distortion arising from out-of-plane movement of the spinal tissues. We observed that the motion distortion could be further mitigated by positioning the animal such that the myelin fibers are parallel to the fast-scan direction of the laser scanning unit. By sufficient reduction of motion distortion, individual nodes of Ranvier could be resolved [Fig. 1(d)]. Multimodal CARS imaging of
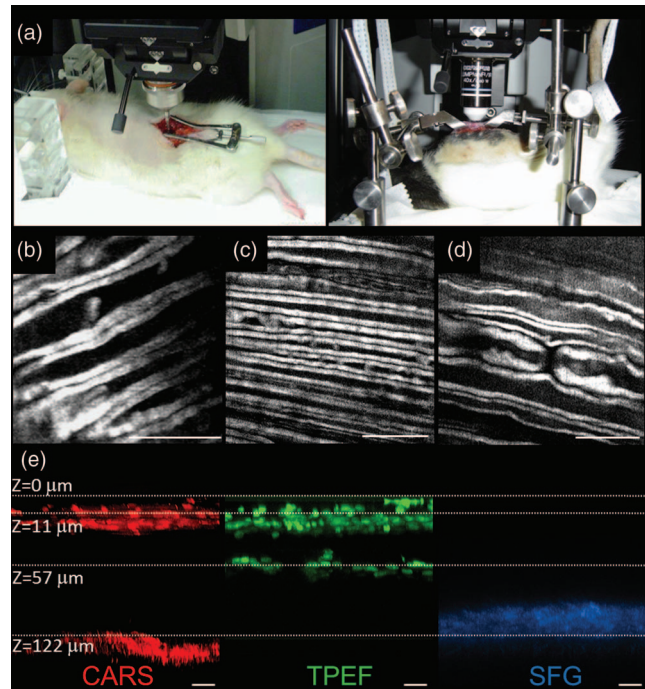

Fig. 1 *In vivo* multimodal CARS imaging of a rats spinal cord. (a) *In vivo* imaging of a spinal cord with a MPO (left panel) and a $40\times$ dipping objective lens (right panel**)**. (b) and (c) *In vivo* CARS image of the superficial dorsal funiculus with (b) MPO and (c) $40\times$ water immersion objective with 3.3 mm working distance. (d) *In vivo* CARS image of node of Ranvier. (e) XZ imaging by CARS (red), TPEF (green), and SFG (blue) reveals that optical penetration is unhindered by spinal cord meninges which allows imaging of myelin fibers $\sim$120 μm under the dura surface. The CARS signal diminishes at c.a. 30 μm from the surface of the white matter. Bar = 20 μm in all images. (Video 1, WMV, 18.3 MB) [URL: http://dx.doi.org/10.1117/1.3641988.1]

white matter, two-photon excited fluorescence (TPEF) imaging of Hoechst labeled cell nuclei, and sum-frequency generation imaging of collagen fibrils in the spinal meninges [Fig. 1(e)] show that our CARS microscope is able to penetrate through the entire dura and map single myelinated axons on the surface of the spinal cord. Because of the curvature of the spinal tissue it is difficult to maintain fluid contact between the tissue and the objective used for CARS imaging. The construction of an agarose well can prevent solution from running off the tissues.

Following a laminectomy, the spinal cord is typically covered with subcutaneous fat to protect the spinal tissue during recovery of the animal, but this procedure is not compatible with longitudinal imaging as reopening the laminectomy site after 1 week revealed that the fat tissue adhered to the dura mater and removal of this tissue often resulted in damage to the spinal tissues. To overcome the complexities presented, we deposited a cushion of agarose gel above the spinal cord after the first imaging procedure. Reopening the laminectomy site 1 week later revealed that a layer of subcutaneous fat had grown above the gel. Removal of the fat layer showed that the agarose cushion remained intact and after careful extraction of the gel with fine forceps, the spinal cord was clearly visible. Subsequent CARS imaging revealed that the spinal cord was covered with a thin layer of red blood cells, deposited during surgery, which effectively blocked
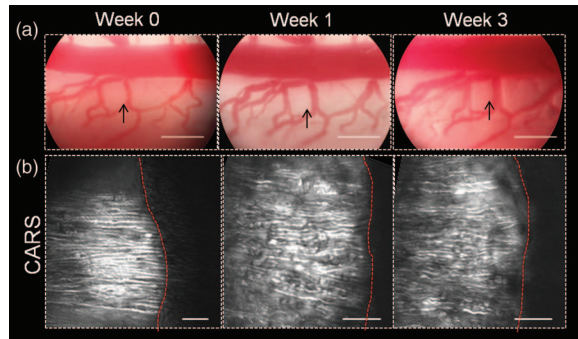
Fig. 2 Longitudinal photography and CARS imaging of the spinal cord white matter in a live rat. (a) Photographs taken at the eyepiece of an upright microscope recorded the general conformation of blood vessels as a landmark following 3 weeks. Arrowheads show the imaging area in (b). Bar = 500 μm. (b) CARS imaging did not show significant myelin damage over the 3 weeks in a rat injected with saline beneath dura. Right to the red dashed lines is the adjacent blood vessel. Bar = 20 μm.

CARS imaging of the white matter. Clearance of these cells by incubation with red blood cell lysis buffer (8.3 g NH_4Cl, 1.0 g $KHCO_3$, 1.8 ml of 5% ethylenediamine tetra-acetic acid in 1 L deionized water) allowed high-resolution CARS imaging of parallel myelin fibers. The application of an agarose barrier and lysis of red blood cells permitted longitudinal imaging of the same region of the spinal cord white matter for a period of 3 weeks (Fig. 2). To ensure repetitive imaging of the same region, we took photos with a digital camera at the eyepiece of the upright microscope to register the conformation of blood vessels that surrounded the area of interest [Fig. 2(a)]. Furthermore, we labeled a small area of the dura mater with a fluorescent probe (Mito-Tracker Green, Invitrogen, Carlsbad, California) to confirm the same region. Repetitive imaging of healthy rats was performed as control. No myelin damage was observed by CARS imaging during the 3-week period [Fig. 2(b)]. Functionally, the animals were evaluated weekly by the Basso, Beattie, Bresnahan[10] scores on a 0 to 21 scale, with 21 indicating no deficit in locomotor function. All animals scored 21 during the 3-week period, which further confirmed no damage to the white matter. The lack of damage is largely because we kept the dura intact during the surgery.

To show the applicability of *in vivo* CARS imaging to studies of myelin pathology and repair, we performed longitudinal imaging of myelin degradation and regeneration after focal demyelination induced by intraspinal injection of $sPLA_2$-III. Twenty-four hours after $sPLA_2$-III injection,[19] myelin breakdown in the form of myelin vesicles was observed throughout the injection site [Fig. 3(a) left]. One week after injection, myelin debris appeared to have been engulfed by infiltrating macrophages and/or microglia [Fig. 3(a), middle]. By 3 weeks post-injection, thinly myelinated axons were visible at the injection site and TPEF imaging of ethidium bromide (5 μM, Invitrogen) labeled of cell nuclei showed elongated nuclei adjacent to some axons, indicative of remyelination by Schwann cells [Fig. 3(a), right]. To ensure what we observed is a remyelination process, NF160 was employed to label the spinal tissues extracted at 1 week after $sPLA_2$ treatment. Nude axons with NF160 labeling but no CARS signal from myelin were extensively observed at the $sPLA_2$ injection site [Fig. 3(b)]. For axons of the same diameter, the measured full width at half maximum
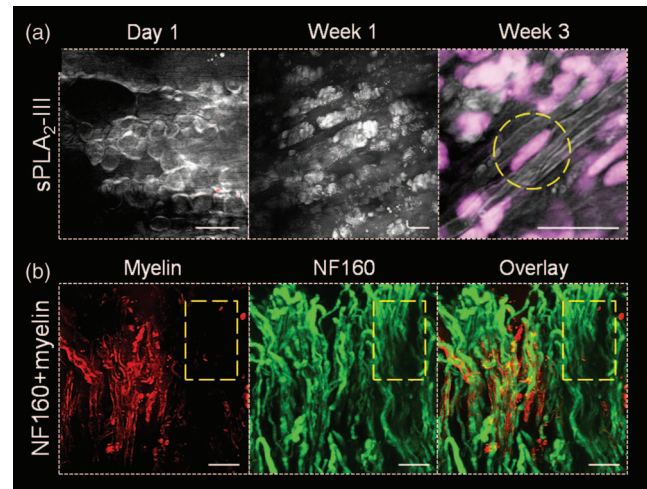

Fig. 3 Longitudinal CARS imaging of $sPLA_2$-III induced demyelination and spontaneous remyelination in a live rat spinal cord. (a) After $sPLA_2$-III injection, myelin degradation was observed in 24 h by formation of myelin vesicles. These vesicles appear to be digested by macrophages/microglia 1 week after injection. By 3 weeks post-injection, signs of Schwann cell mediated remyelination were visible, with elongated cell nuclei (dashed circle) adjacent to myelinated axons at the injection site. (b) At 1 week post $sPLA_2$-III injection, the myelin sheath was visualized by CARS (red), axons were visualized by immunofluorescent staining of NF160 (green). The overlay image showed the absence of myelin sheath (dashed square). Bar = 20 μm in all images.

of the remyelinated sheaths was 0.71 ± 0.05 μm, thinner than that of the control group, 0.89 ± 0.06 μm, possibly because the new myelin is contributed by Schwann cells. These data show that CARS microscopy is able to monitor subtle changes to myelin *in vivo*.

A potential application of longitudinal CARS imaging is to monitor white matter injury and repair after a traumatic spinal cord injury. Traumatic injury to the spinal cord results in the disruption or loss of myelin,[5] and functional deficit following SCI has been directly correlated with the degree of demyelination.[21] Developing strategies to promote remyelination of axons is therefore a critical requirement for restoration of axon conduction and improving locomotor function. Nevertheless, limited information regarding the response of CNS to myelinating cells has hindered the translation of remyelination treatments to clinical settings. By monitoring the activities and outcome of implanted cells, longitudinal *in vivo* CARS imaging opens up new opportunities for the rational development of myelin repair therapies.

Acknowledgments

References

1. M. J. Levene, D. A. Dombeck, K. A. Kasischke, R. P. Molloy, and W. W. Webb, "*In vivo* multiphoton microscopy of deep brain tissue," *J. Neurophysiol.* **91**, 1908–1912 (2004).

2. B. A. Sabel, R. Engelmann, and M. F. Humphrey, "*In vivo* confocal neuroimaging (ICON) of CNS neurons," *Nat. Med.* **2**, 244–247 (1997).

3. M. Kerschensteiner, M. E. Schwab, J. W. Lichtman, and T. Misgeld, "*In vivo* imaging of axonal degeneration and regeneration in the injured spinal cord," *Nat. Med.* **11**, 572–577 (2005).

4. C. Dray, G. Rougon, and F. Debarbieux, "Quantitative analysis by *in vivo* imaging of the dynamics of vascular and axonal networks in injured mouse spinal cord," *Proc. Natl. Acad. Sci. U.S.A.* **106**, 9459–9464 (2009).

5. M. O. Totoiu and H. S. Keirstead, "Spinal cord injury is accompanied by chronic progressive demyelination," *J. Comp. Neurol.* **486**, 373–383 (2005).

6. M. Stangel and H. P. Hartung, "Remyelinating strategies for treatment of multiple sclerosis," *Prog. Neurobiol.* **68**, 361–376 (2002).

7. M. E. Schwab, "Repairing the injured spinal cord," *Science* **295**, 1029–1031 (2002).

8. S. Thuret, L. D. F. Moon, and F. H. Gage, "Therapeutic interventions after spinal cord injury," *Nat. Rev. Neurosci.* **7**, 628–643 (2006).

9. A. R. Blight, "Delayed demyelination and macrophage invasion: a candidate for secondary cell damage in spinal cord injury," *Cent. Nerv. Syst. Trauma.* **2**, 299–315 (1985).

10. D. M. Basso, M. S. Beattie, and J. C. Bresnahan, "A sensitive and reliable locomotor rating scale for open field testing in rats," *J. Neurotrauma* **12**, 1–21 (1995).

11. H. Bridge and S. Clare, "High-resolution MRI: *in vivo* histology?," *Philos. Trans. R. Soc. Lond. B Biol. Sci.* **361**, 137–146 (2006).

12. B. Stankoff, Y. Wang, M. Bottlaender, M. S. Aigrot, F. Dolle, C. Wu, D. Feinstein, G. F. Huang, F. Semah, C. A. Mathis, W. Klunk, R. M. Gould, C. Lubetzki, and B. Zalc, "Imaging of CNS myelin by positron-emission tomography," *Proc. Natl. Acad. Sci. U.S.A.* **103**, 9304–9309 (2006).

13. L. Li, H. Wang, and J. X. Cheng, "Quantitative coherent anti-Stokes Raman scattering imaging of lipid distribution in coexisting domains," *Biophys. J.* **89**(5), 3480–3490 (2005).

14. Y. Fu, H. Wang, T. B. Huff, R. Shi, and J.-X. Cheng, "Coherent anti-Stokes Raman scattering imaging of myelin degradation reveals a calcium dependent pathway in Lyso-Ptd-Cho induced demyelination," *J. Neurosci. Res.* **85**, 2870–2881 (2007).

15. Y. Fu, W. Sun, Y. Shi, R. Shi, and J.-X. Cheng, "Glutamate excitotoxicity inflicts paranodal myelin splitting and retraction," *PLoS ONE* **4**, e6705 (2009).

16. T. B. Huff and J.-X. Cheng, "*In vivo* coherent anti-Stokes Raman scattering imaging of sciatic nerve tissue," *J. Microsc.* **225**, 175–182 (2007).

17. F. P. Henry, D. Côté, M. A. Randolph, E. A. Rust, R. W. Redmond, I. E. Kochevar, C. P. Lin, and J. M. Winograd, "Real-time *in vivo* assessment of the nerve microenvironment with coherent anti-Stokes Raman scattering microscopy," *Plast. Reconstr. Surg.* **123**, 123S–130S (2009).

18. X. Z. Liu, X. M. Xu, R. Hu, C. Du, S. X. Zhang, J. W. McDonald, H. X. Dong, Y. J. Wu, G. S. Fan, M. F. Jacquin, C. Y. Hsu, and D. W. Choi, "Neuronal and glial apoptosis after traumatic spinal cord injury," *J. Neurosci.* **17**, 5395–5406 (1997).

19. W. L. Titsworth, S. M. Onifer, N. K. Liu, and X. M. Xu, "Focal phospholipases A2 group III injections induce cervical white matter injury and functional deficits with delayed recovery concomitant with Schwann cell remyelination," *Exp. Neurol.* **207**, 150–162 (2007).

20. Y. Fu, T. B. Huff, H.-W. Wang, J.-X. Cheng, and H. Wang, "*Ex vivo* and *in vivo* imaging of myelin fibers in mouse brain by coherent anti-Stokes Raman scattering microscopy," *Opt. Express* **16**(24), 19396–19409 (2008).

21. Q. Cao, Y. P. Zhang, C. Iannotti, W. H. DeVries, X. M. Xu, C. B. Shields, and S. R. Whittemore, "Functional and electrophysiological changes after graded traumatic spinal cord injury in adult rat," *Exp. Neurol.* **191**, S3–S16 (2004).